Digital Twin of a Beam Selection Procedure in an Indoor Scenario

Genivaldo Charchar[1], Gabriel Vieira[1], Valdinei Conceição[1], Cleverson Nahum[1], Ilan Correa[1], Silvia Lins[2] and Aldebaro Klautau[1]

***Abstract*— Millimeter Wave (mmWave) communications, vital for 5G/6G, addresses sub-6 GHz congestion but needs directional beamforming due to high path loss. Machine Learning (ML) for beam selection faces scarce indoor training data for creating robust ML models. A by-product of Digital Twin (DT) frameworks is the generation of realistic synthetic datasets, which help training ML models. This work presents and validates a methodology to construct accurate DT from low-cost radio measurements. A DT of an indoor mmWave multiple input single output (MISO) system, using Wireless Insite ray tracing, was developed. It achieved 100% top-1 beam accuracy and strong received signal strength correlation in line-of-sight conditions.**

***Keywords*— Beam selection, channel modeling, millimeter-wave, MIMO, ray-tracing, RSS.**

I. Introduction

Wireless communication, enabled by 5G and emerging 6G technologies, is key to supporting high data rates, low latency, and massive connectivity, especially in dense and mobile settings. Due to the limited availability of sub-6GHz spectrum, Millimeter Waves (mmWave) have gained prominence for offering wide bandwidth and enabling compact device designs, despite their susceptibility to higher path loss and signal fading [1]. To address these propagation challenges, Multiple Input Multiple Output (MIMO) architectures are essential in 5G systems, especially those employing beamforming techniques. By focusing energy in specific directions, beamforming enhances signal strength, improves link reliability, and increases spectral efficiency, making it crucial strategy for effective communication at high-frequency mmWave bands [2].

Measurement campaigns using beamforming transceivers build datasets for training Machine Learning (ML) models for beam selection [3], but such campaigns are expensive, complex, and resource-intensive. In this context, simulating real-world environments through Digital Twin (DT) becomes a powerful tool to generate more extensive and rapidly executable datasets [4]. A robust alternative is the Ray Tracing (RT) approach, which enables accurate modeling of signal propagation in realistic physical settings, offering reference data for performance evaluation and significantly reducing the need for field measurements.

Recent studies have explored this simulation-based methodology with promising results. For instance, Yuan et al. [5] demonstrated the accuracy of RT simulations in reproducing measured behavior in complex scenarios involving advanced antenna configurations, with a focus on detailed channel modeling for next-generation wireless systems. While their contribution provides valuable insights for channel characterization, our approach differs by using a simplified representation at a fixed frequency. This simplification enables a more direct and practical evaluation of beam selection strategies, using the same antenna configuration and codebook employed in real-world. Complementarily, Jiang et al. [6] use RT-based digital twins to train ML models for beam prediction in mmWave systems, leveraging synthetic environments that capture key spatial features like user position and geometry. Their validation relies on neural network–predicted beam indices at the inference level, whereas we perform physical-layer validation by directly comparing simulated and measured received power, enabling a more rigorous assessment of the Digital Model (DM) accuracy in replicating beam selection behavior.

This paper introduces a foundational methodology for developing DT for beam selection procedure based on data from low-cost radio setups, with the goal of refining the process of constructing DM and addressing the scarcity of training data. The approach focuses on improving the modeling process by incorporating elements from real-world experiments, evaluating the model's ability to reproduce signal variation patterns observed in physical measurements. To this end, we employ a combination of statistical, signal-based, and ranking-based metrics to compare simulated behavior with actual measurements. Results show that while the proposed methodology successfully captures key patterns, further refinements are required to enable robust and scalable digital twin development for future wireless applications.

II. System modeling

In this study, the modeling process is achieved by conducting and evaluating experiments within a static scenario, where data inputs are manually controlled and without real-time synchronization to physical system. This approach is more precisely characterized as a DM [7], as it lacks dynamic, bidirectional synchronism inherent to a fully realized DT.

Our setup, located in a laboratory room, represented at Figure 1, involves measurement campaigns using commercial radios configured in a Multiple Input Single Output (MISO) arrangement. The Base Station (BS) employs a Uniform Planar Array (UPA) with N_{tr} antenna elements dedicated to Real Experiments (RE) and N_{ts} elements for Simulation Experiments (SE), communicating with three single-antenna User

[1]LASSE - Telecommunications, Automation and Electronics Research and Development Center, Federal University of Pará (UFPA), Belém-PA, Brazil. E-mails: {genivaldo.silva, gabriel.vieira, valdinei.conceicao}@itec.ufpa.br; {cleversonahum, ilan, aldebaro}@ufpa.br; [2]Innovation Center, Ericsson Telecomunicações S.A., Brazil. E-mail:silvia.lins@ericsson.com

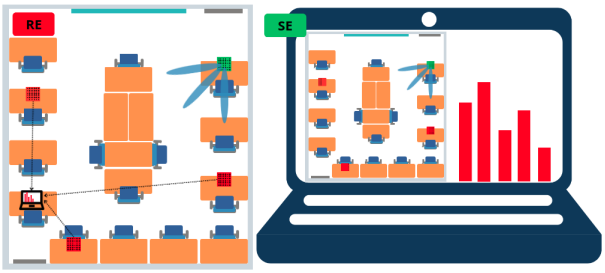

Fig. 1. Beam selection on DM of indoor scenario.

Equipments (UEs)s and these measurements are conducted at a mmWave carrier frequency of f_c. In parallel with the measurements, we simulate the electromagnetic propagation within a digital model of this room. For that, we employ the Wireless Insite (WI) RT simulator (v3.4.5) to implement SE. WI simulates accurately reflection, diffraction, scattering, fading and absorption, with a set of rays launched from the transmitter, each characterized by gain, phase, Angles of Departure (AoD), and Angle of Arrival (AoA) in spherical coordinates (azimuth ϕ and zenith θ), used for total ray gain calculation, by combining antenna patterns and path gain.

The channel model in SE initially yields a $N_{ts} \times 1$ channel matrix ($\mathbf{H}$) per UEs. This corresponds, via precoding, to the $(N_{tr}) \times 1$ effective channel representation relevant to the active antenna elements used in the RE. Each element of the matrix represents the complex propagation factor $\mathbf{g}_k = \sqrt{G_k} e^{i\theta_k}$ for a specific Transmitter (Tx)-Receiver (Rx) antenna pair. Here, G_k denotes the power gain from the transmit element to receive element k, and θ_k represents the corresponding phase shift. The complete structure of the channel matrix ($\mathbf{H}$-matrix), incorporating these factors, is given by

$$\mathbf{H} = [\mathbf{g}_1^*, \mathbf{g}_2^*, .., \mathbf{g}_k^*], \tag{1}$$

where * denotes the conjugate transpose operation [8].

Beamforming at the BS uses a codebook of N_c codewords ($N_{tr} \times N_c$ for RE, $N_{ts} \times N_c$ for SE). In SE, corner antenna deactivation is modeled using zero magnitude entries and row-major index remapping to match the BS setup. The combined channel, given by

$$\mathbf{y}_i = \mathbf{H}\mathbf{f}_i, \tag{2}$$

results from applying the precoding vector $\mathbf{f}$ (from the codebook) to the $\mathbf{H}$-matrix. For SE evaluation, a 1 mW transmit power is assumed for this combined channel, with results converted to dBm. The main focus is beam selection, which involves choosing the best beam from the N_c predefined codebook options based on the highest Received Signal Strength (RSS). This optimal beam index i is determined by

$$\hat{i}_{optimal} = \underset{i \in \{1,\ldots,N_c\}}{\arg\max} |y_i|. \tag{3}$$

Finally, in the RE, the required RSS values for this selection process are obtained by converting measured Received Signal Strength Indicator (RSSI) according to [9], where

$$\text{RSS} = 0.0651 \cdot \text{RSSI} - 74.3875. \tag{4}$$

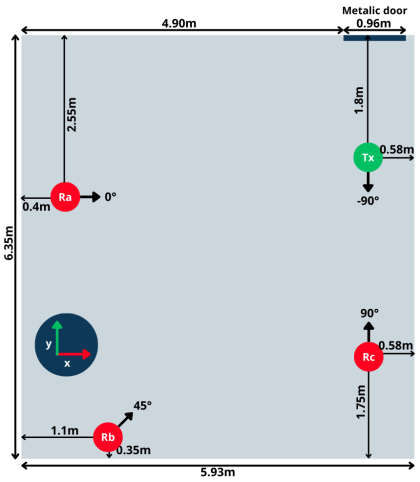

Fig. 2. Room layout showing dimensions, BS/UE radio positions and UPA orientations.

III. Measurements and RT Simulation Campaigns

To validate the proposed beam selection approach based on $\mathbf{H}$-matrix data from WI, MIMO channel measurements were carried out along with their simulated equivalents. These measurements aimed to provide a reliable ground truth for assessing the accuracy and effectiveness of the simulated results. This section presents the measurement setup, the corresponding DM used and the post-processing applied for comparative analysis.

A. Real Environment

Mikrotik wAP 60G radios (IEEE 802.11ad) were used for data acquisition during the measurement campaign in a meeting room with the original furniture arrangement preserved to ensure environmental realism. BS and UEs were positioned at the same height, with the BS's UPA boresight oriented $90°$ clockwise. The UEs was evaluated at three positions: in the boresight Line-of-Sight (LoS) scenario, R_C (closest to BS, UPA boresight $90°$ counterclockwise) and R_B in off-boresight LoS (farther from BS, UPA boresight $45°$ counterclockwise); and in multipath-dominant LoS scenario, R_A (UPA facing the positive x-axis), as illustrated in Figure 2. Furthermore, the BS employed a UPA composed of $N_{tr} = 36$ antenna elements in a 6×6 configuration, with four corner elements disabled. To suppress back radiation, a metallic plate was placed behind the array, while each element was a dual-polarized crossed dipole, providing diversity and multipath robustness. The system uses a client-server architecture where a central Orchestrator manages clients and data acquisition and reception. In this setup, the clients, comprising radios operating in Station (STA) mode, capture RSSI and transmit the measurements to the server. Based on the reported RSSI values, the RSS parameter (defined in Eq. 4) is computed and then used to find the optimal beam pair. For operation, the system requires at least one radio configured in Access Point (AP) mode and another in STA mode. Beside, to prevent data inconsistencies during beam sweeping, the RSSI sampling interval was fixed at $200\,ms$. Finally, due to the static nature of the measurement environment and the low variability across

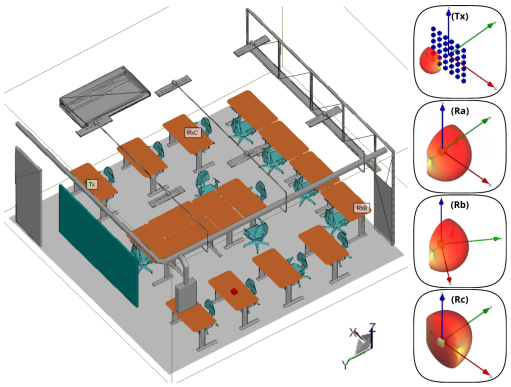

Fig. 3. Representation of the real scenario as a 3D model within the WI simulation software and dipole radiation pattern.

samples, each data collection consisted of 50 RSSI readings. The average of these values was then extracted and used for the beam selection analysis.

B. Digital Environment

The 3D environment in Figure 3 was modeled in Blender, accurately aligned with real-world dimensions. However, to simplify the scene and reduce computational cost, certain objects were removed or had their mesh complexity reduced by decreasing the number of faces. For the simulation itself, the widely adopted RT tool WI was utilized, as its comprehensive features enable highly accurate reproduction of the real environment's physical characteristics. Within this simulation framework, the electromagnetic properties of materials were assigned according to International Telecommunication Union (ITU) recommendations at $f_c = 60GHz$ [10], while the X3D propagation model was employed to consider multiple wave interactions with the environment. Besides, simulation configurations, including Tx and Rx positions, the UPA layout at the Tx side ($N_{ts} = 36$), and operating frequency, were set to replicate the measurement campaign conditions.

Although the measurements utilized crossed dipoles, a simplified model employing a single vertically polarized dipole was adopted for each antenna element in the RT simulation. This simplification was necessary due to the inherent challenges in exporting the more complex radiation pattern of the measurement's crossed dipoles into the WI software, with the gain of this simulated dipole model being dependent on antenna type and orientation. Additionally, to accurately account for the reflective effects from the metallic plate behind the actual MikroTik UPA and thereby replicate the observed suppression of back radiation, these simulated dipole antennas were configured to radiate only within the 180° to 360° azimuthal range. A comprehensive summary comparing the configurations adopted in both the measurement and RT simulation campaigns is provided in Table I.

C. Post-processing: Codebook Implementation

$\mathbf{H}$-matrix is generated according to the procedure described in Eq. 1, and subsequently exported to the main processing script, where the equivalent channel is constructed as described in Eq. 2. This equivalent channel incorporates the same codebook with $N_c = 64$ used by the physical antenna array. Finally, two key pieces of information are extracted from the equivalent channel: the received power corresponding to each beam pair, obtained from the magnitude of the equivalent channel, as well as the selected beam pair at the three receiver positions defined in Eq. 3. In the subsequent sections will be present and compare the results obtained from both campaigns to validate the overall performance.

TABLE I
CONFIGURATIONS IN MEASUREMENTS & RT SIMULATIONS

Parameter	Value
Common	
Operating frequency	60.48 GHz
Tx and Rx height	0.70 m
Transmit array (Tx)	6×6 UPA (36 elements, 4 disabled)
Receive antenna (Rx)	Single element
Beamforming method	Beam sweeping
Measurements	
Hardware	MikroTik wAP 60G
Standard	IEEE 802.11ad [11]
Antenna type	Crossed-dipole
Antenna polarization	Dual (Vertical+Horizontal)
Measurement duration	50 s (250 samples)
RSS sampling interval	200 ms
RT Simulations	
Simulation tool	Wireless InSite
Antenna type	Dipole
Antenna polarization	Vertical
Propagation model	X3D
Material database	ITU Rec. [10]
Max interactions	6 reflections, 1 diffraction

IV. VALIDATION RESULTS

This section compares measured RSS values with simulated equivalent channel magnitudes under boresight LoS, off-boresight LoS and multipath-dominant LoS conditions. The performance of the DM approach is then evaluated using 4 key metrics. The Pearson Correlation Coefficient (PCC) is employed to quantify the linear relationship between the RSS distributions observed in the real and simulated scenarios, the RSS Mean Absolute Error (MAE) between SE and RE of each Rx is compared to each other to quantify impact of Rx position change on results of approaches used. Top-K beam selection accuracy is assessed by comparing beam selections in the real environment versus those in the simulated environment, while Precision@K measures the proportion of Top-K correctly predicted beams in SE using Top-K from RE as ground truth to evaluate overall ranking fidelity.

TABLE II
ERROR AND CORRELATION OVER SE TO RE

Receiver	$\mathbf{R_A}$	$\mathbf{R_B}$	$\mathbf{R_C}$
MAE (dBm)	3.145	2.233	3.436
STD (dBm)	2.708	1.747	2.316
Normalized MAE	2.739×10^{-1}	1.286×10^{-1}	1.621×10^{-1}
PCC	1.767×10^{-1}	4.256×10^{-1}	6.605×10^{-1}
ρ-value	1.625×10^{-1}	4.553×10^{-4}	2.872×10^{-9}

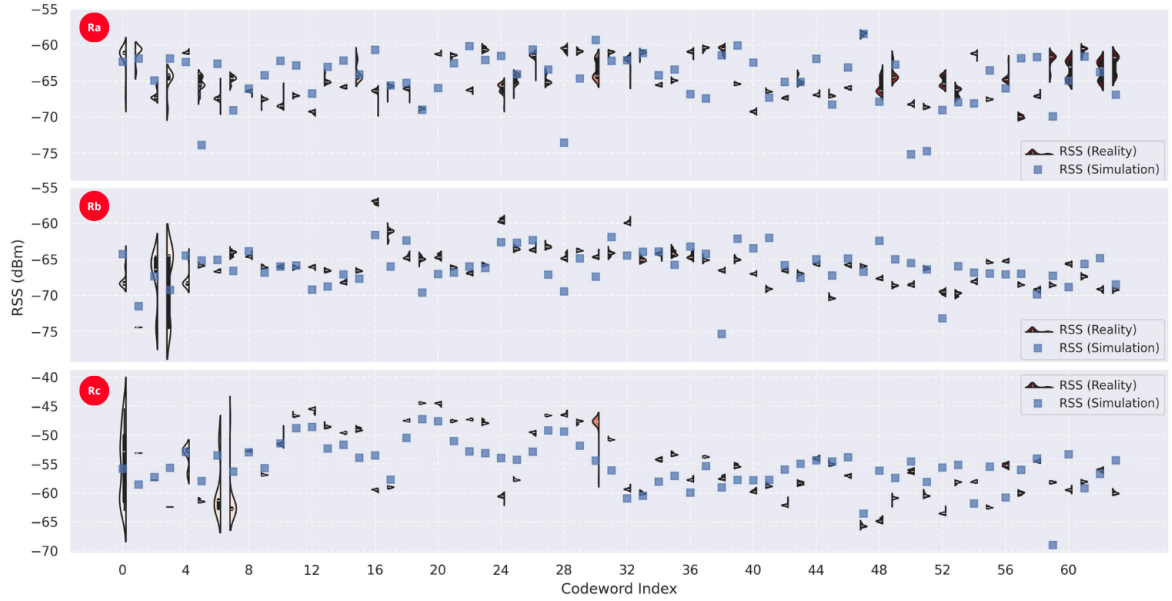

Fig. 4. Comparison of RE (violin plot with 50 sample per codeword) and SE RSS on receivers by codeword index.

A. RSS Distribution Analysis

To assess the linear correlation between the RSS distributions from the real and simulated scenarios across all 64 beams, we employed the PCC [12]. Table II presents the calculated PCC values and their corresponding ρ-values for each receiver, considering a significance level of 99% to reject the null hypothesis (H_0), where linear correlation is zero. For this, the RSS from real measurements (obtained by averaging 50 samples per beam) was correlated with the corresponding single simulated RSS value for each beam. Although the receiver R_A, under multipath-dominant LoS, showed a weak correlation and not sufficient statistic evidence to reject H_0, receiver R_C (favorable condition), demonstrated a strong correlation, while R_B, with a off-boresight LoS and located farther from the Tx, exhibited a moderate correlation, both with sufficient statistic evidence to reject H_0. Figure 4 visually supports these distributional comparisons, displaying measurement data via violin plots (showing 50-sample variation) alongside simulated channel magnitudes converted to dBm (assuming $0\,dBm$ Tx power for this visualization). While measured data shows greater variability (evident in violin plots, potentially from channel/equipment effects), simulated values align well with measurement medians, indicating effective capture of underlying signal strength trends. Due to a significant mean difference between absolute measured and simulated values, an approximate $-23.5\,dBm$ offset—derived from the overall MAE between their average RSS—was applied to the DM data. This adjustment aligns their means, facilitating a more effective relative comparison and qualitative validation. Further quantitative assessment, provided in Table II, includes MAE, Standard Deviation (STD) of the error and normalized MAE (defined as MAE divided by the RE RSS range per Rx). The normalized MAE for receiver R_A is approximately twice that of R_B and R_C, which show similar alignment with RE. Despite using the same scenario and methodology to measure RSS across receivers, differences in receiver position affect path gain and antenna pattern gain via AoD and AoA. Given the LoS conditions, scenario-related discrepancies are minimal. Thus, the significant MAE disparity for R_A likely stems from SE antenna radiation pattern, adversely impacted by R_A's sidelong position relative to the transmitter.

B. Beam Selection

To evaluate the DMs beam prediction performance, we use Top-K accuracy [13] and Precision@K. Top-K accuracy describe if the optimal beam index from RE is in the Top-K predicted beam set from SE, while Precision@K measures the proportion of Top-K correctly predicted beams in SE, B_K^{SE}, relative to the RE Top-K ground truth set, B_K^{RE}. The concept is similar to precision metric described in [14], where true positives number is divided by all assigned as positive, but here true positive is the number of beam index present in both sets, and the number of all positives is the set length, Top-K indices. It is obtained by

$$\text{Precision@k} = \frac{|B_K^{SE} \cap B_K^{RE}|}{K} \times 100\%, \tag{5}$$

where $|\cdot|$ denotes set cardinality. First, each receiver has its beams ranked by decreasing equivalent channel magnitude (SE) and average measured RSS from samples (RE). From these rankings, Top-K and Precision@K results are obtained.

Top-1 accuracy was 100% for all receivers, that is, single best simulated beam matched the best real beam, but this metric provides limited insight into overall ranking fidelity. To further evaluate performance, we analyzed Precision@K, as shown in Figure 5. This metric compares the set of Top-K indices from the SE with those from the RE, bench marked against a 'dummy' line representing random selection. For R_A, Precision@K indicated that only the optimal beam was common to both sets for K values from 1 up to 7. Its proximity to the dummy baseline suggests challenging propagation

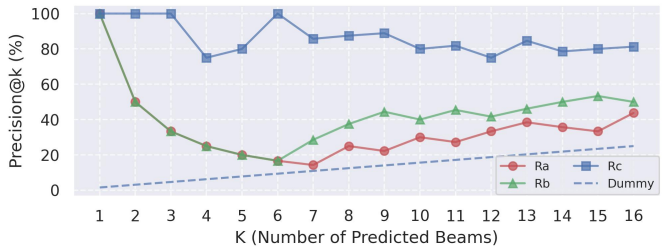

Fig. 5. Precision@K from each receiver over Top-K predicted beams.

conditions. This could be attributed to inaccuracies in the simulated antenna radiation pattern approach, limitations of the codebook's angular coverage, or R_A's less favorable, oblique position relative to the Tx. R_B's Precision@K behavior was initially similar to R_A's but showed improved performance beyond K=6. This might indicate that the chosen antenna radiation pattern model was a slightly better fit for R_B's diagonal position. In contrast, R_C initially achieved 100% Precision@K, indicating perfect rank agreement for the top beams. A dip at K=4, followed by a return to 100% at K=6, highlights minor ranking mismatches. However, R_C's overall performance remained consistently high (around 80% or above), likely due to its favorable position directly in front of the Tx. Comparing receivers results to each other, it was observed increase of ranking mismatches as the angle of Rx position relative to Tx normal grew. These results underscore the significant impact of receiver positioning and antenna modeling fidelity on beam prediction accuracy. However, even under unfavorable conditions, the simulation model successfully identified the same optimal beam as determined from the real measurements in all cases.

V. Conclusions

The objective of this work was to advance towards comprehensive DT by developing and validating a methodology for building accurate DMs derived from low-cost radio setups based on RT—envisioned as a key component for a future DT capable of operating in dynamic, mobile environment—by comparing its predictions against real-world measurements, using the Top-K beam selection accuracy, Precision@K, normalized MAE and PCC (all based on RSS) as the main performance indicators at this initial stage. PCC results demonstrated a strong correlation in the RSS distribution across all beams between the model and measurements under boresight LoS condition, at top-1 all receivers achieved 100% accuracy, Precision@K showed overall ranking fidelity, where ranking mismatches increased as the angle of the receiver position relative to the transmitter direction increased, normalized MAE comparison between receivers suggest approach antenna radiation pattern as dipole was the cause. Notably, these outcomes were achieved despite simplifications in modeling the scenario and, crucially, the antenna radiation patterns (single dipole vs. crossed dipole). Furthermore, the RT model consistently underestimated path loss compared to real-world measurements, what points to inaccurate setting of Tx transmission power. Actual work requires refined calibration for accurate absolute power estimates, such as the applied average MAE offset. Future works should focus on mitigating current model limitations by, for example, incorporating a more accurate antenna radiation pattern (such as crossed dipole), accurately setting the Tx transmission power to improve its radio characterization within the digital model, and evaluating performance in scenarios where directivity benefits are more pronounced. Additionally, investigating the approach of simulating a Single Input Single Output system via RT followed by post-processing to generate MISO results could be explored to reduce simulation time for potential real-time DT applications.

Acknowledgements

This study was financed in part by the Coordenação de Aperfeiçoamento de Pessoal de Nível Superior - Brasil (CAPES) – Finance Code 001; the Conselho Nacional de Desenvolvimento Científico e Tecnológico (CNPq); the Brasil 6G project (01245.020548/2021-07), supported by RNP and MCTI; the Innovation Center, Ericsson Telecomunicações S.A., Brazil; OpenRAN Brazil - Phase 2 project (MCTI grant Nº A01245.014203/2021-14); Project Smart 5G Core And MUltiRAn Integration SAMURAI (MCTIC/CGI.br/FAPESP under Grant 2020/05127-2).

References

[1] W. Chen *et al.*, "5G-Advanced Toward 6G: Past, Present, and Future," *IEEE Journal on Selected Areas in Communications*, vol. 41, no. 6, pp. 1592–1619, 2023.

[2] S. Rangan, T. S. Rappaport, and E. Erkip, "Millimeter-Wave Cellular Wireless Networks: Potentials and Challenges," *Proceedings of the IEEE*, vol. 102, no. 3, pp. 366–385, 2014.

[3] A. Oliveira, D. Suzuki, S. Bastos, I. Correa, and A. Klautau, "Machine Learning-Based mmWave MIMO Beam Tracking in V2I Scenarios: Algorithms and Datasets," in *IEEE Latin-American Conf. on Commun. (LATINCOM)*, pp. 1–5, 2024.

[4] O-RAN Alliance, "Digital Twin RAN: Key Enabling Technologies Research Report," tech. rep., O-RAN ALLIANCE, 2023.

[5] Z. Yuan, J. Zhang, V. Degli-Esposti, Y. Zhang, and W. Fan, "Efficient Ray-Tracing Simulation for Near-Field Spatial Non-Stationary mmWave Massive MIMO Channel and Its Experimental Validation," *IEEE Trans. on Wireless Commun.*, vol. 23, no. 8, pp. 8910–8923, 2024.

[6] S. Jiang and A. Alkhateeb, "Digital Twin Based Beam Prediction: Can We Train in the Digital World and Deploy in Reality?," in *IEEE International Conf. on Commun. Workshops*, pp. 36–41, 2023.

[7] W. Kritzinger, M. Karner, G. Traar, J. Henjes, and W. Sihn, "Digital Twin in Manufacturing: A Categorical Literature Review and Classification," *IFAC-PapersOnLine*, vol. 51, no. 11, pp. 1016–1022, 2018.

[8] Remcom Inc., *Wireless InSite 3.3.0 User Manual*, 2018. Chapter 21, Section 1.3.

[9] Y. Song, C. Ge, L. Qiu, and Y. Zhang, "2ACE: Spectral Profile-driven Multi-resolutional Compressive Sensing for mmWave Channel Estimation," *Proceedings of the 4th ACM Workshop on Millimeter-Wave and Terahertz Networks and Sensing Systems*, pp. 7–12, 2023.

[10] R. S. I.-R. International Telecommunication Union, "Effects of building materials and structures on radiowave propagation above about 100 MHz," Recommendation ITU-R P.2040-1, International Telecommunication Union, July 2015. Available at: https://www.itu.int/rec/R-REC-P.2040-1-201507-I/en.

[11] R. S. I.-R. International Telecommunication Union, "IEEE Standard for Wireless LAN Medium Access Control (MAC) and Physical Layer (PHY) Specifications Amendment 3: Enhancements for Very High Throughput in the 60 GHz Band," Standard IEEE Std 802.11ad-2012, IEEE, 2012.

[12] F. J. Gravetter and L. B. Wallnau, *Statistics for the Behavioral Sciences*, ch. 15, pp. 489–509. Boston, MA: Cengage Learning, 10 ed., 2017.

[13] 3GPP, "TR 38.843: Study on Artificial Intelligence /Machine Learning for NR Air Interface," technical report, 3rd Generation Partnership Project, Technical Specification Group Radio Access Network, 2023.

[14] C. D. Manning, P. Raghavan, and H. Schütze, *Introduction to Information Retrieval*. Cambridge University Press, 2008.